Joule

CellPress

Article

Chelated Chromium Electrolyte Enabling High-Voltage Aqueous Flow Batteries

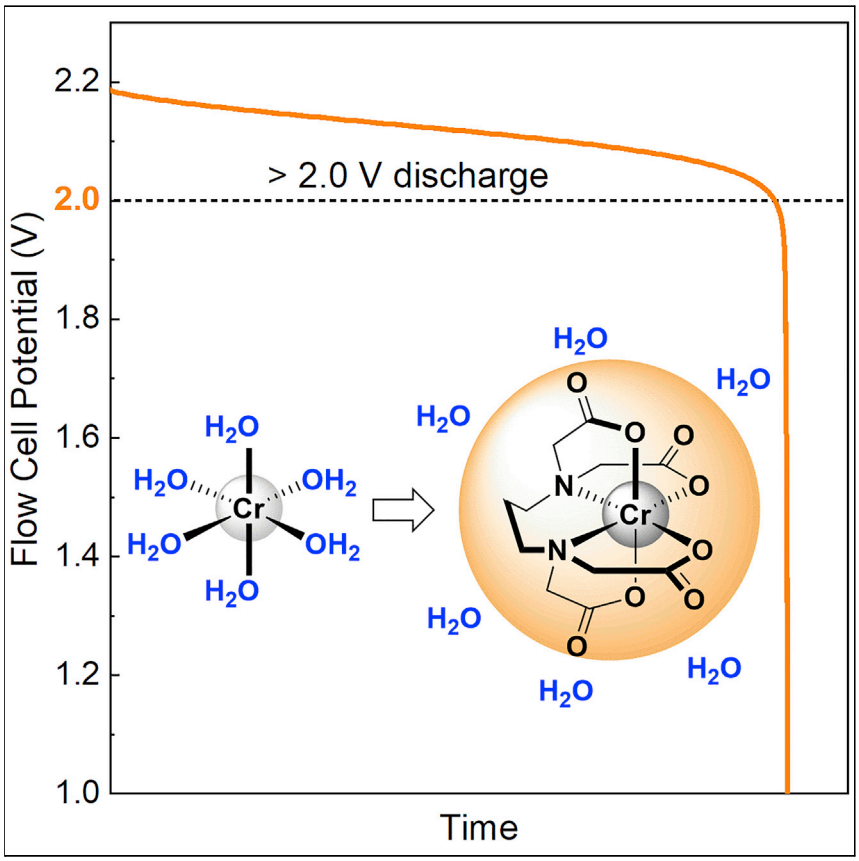

This work demonstrates two high-voltage aqueous flow batteries, including one operating at a non-hybrid record 2.13 V cell potential. These batteries utilize a negative electrolyte comprised of chelated chromium ions and operate near neutral pH with high efficiency. The chelate acts as a solvent barrier or "molecular SEI," inhibiting water splitting by the highly reducing Cr^{2+} ion. The combination of earth abundant redox-active metals and mass-produced organic chelates represents a compelling direction for low-cost flow battery electrolyte chemistry.

Brian H. Robb, Jason M. Farrell, Michael P. Marshak

michael.marshak@colorado.edu

HIGHLIGHTS

Two of the highest voltage all-aqueous flow batteries operate near neutral pH

Chelation inhibits H_2 evolution, shattering established aqueous operating window

Exploits the versatility of organics and stability of metal-centered redox

Mass-produced materials enable low-cost electrolyte and facilitate scale-up

Robb et al., Joule 3, 2503–2512
October 16, 2019
https://doi.org/10.1016/j.joule.2019.07.002

Joule

CellPress

Article

Chelated Chromium Electrolyte Enabling High-Voltage Aqueous Flow Batteries

Brian H. Robb,[2] Jason M. Farrell,[2] and Michael P. Marshak[1,3,4,*]

SUMMARY

Widespread adoption of renewable energy is limited by the lack of low-cost long-duration energy storage. Redox flow batteries are an attractive option to provide this type of storage because their power and energy components can be scaled independently; however, systems commercialized to date have failed to realize this low-cost potential, primarily because of the cost and performance of the battery chemistry. Here, we resolve these challenges with a negative electrolyte comprised of earth-abundant chromium and an inexpensive chelating agent which operates at a more reducing potential than zinc while inhibiting hydrogen production. Utilizing this electrolyte, we report two of the highest voltage aqueous flow batteries, which have stably operated at room temperature and near neutral pH with high efficiency and high power density. These results demonstrate the ability of chelated metal complexes to prevent water coordination and establish a general method for inhibiting water splitting reactions at highly negative potentials.

INTRODUCTION

Solar and wind have become the least expensive forms of new power generation in the United States, but their intermittent nature coupled with the lack of available low-cost energy storage limits their wide-scale adoption.[1] Redox flow batteries (RFBs) are considered to be a promising technology to provide long-duration stationary energy storage at grid-scale.[2,3]

The iron-chromium (FeCr) RFB was among the first chemistries investigated because of the low cost and large abundance of chromite ore.[3,4] Although the FeCr electrolyte cost is low, challenges associated with FeCr flow batteries include low cell voltage (1.2 V), low current densities (21.5 mA cm^{-2}) due to sluggish $Cr^{3+/2+}$ redox kinetics, required operation in corrosive HCl solution for metal ion solubility, permeability of metal ions through membranes, and hydrogen gas evolution.[5,6] In contrast, the all-vanadium RFB operates at a higher voltage (1.4 V), higher current density ($\geq$100 mA cm^{-2}), and the use of aqueous vanadium ions for both negative and positive electrolyte enables periodic rebalancing to mitigate metal ion crossover, but requires the use of expensive vanadium and corrosive sulfuric acid.[7,8]

The use of metal chelates, including those employing chromium[9–11] and iron,[12–16] has been investigated for RFB electrolytes, enabling the manipulation of redox potential, solubility, and solution electrolyte pH, as well as mitigating membrane crossover. In particular, chelating chromium with the ubiquitous chelate ethylenediaminetetraacetic acid (EDTA) has been shown to shift the $Cr^{3+/2+}$ reduction potential from −0.41 to −0.99 V versus the standard hydrogen electrode (SHE) near neutral pH[17] and to enhance the chromium redox kinetics by more than 10^5.[18] A symmetric flow battery

Context & Scale

Redox flow batteries are an attractive option to provide low-cost long-duration energy storage but have failed to realize their low-cost potential, primarily because of the cost and performance of the battery chemistry. Here, we demonstrate an electrolyte comprising earth-abundant chromium ions that are stabilized by an inexpensive chelating agent. This electrolyte enables two of the highest voltage aqueous flow batteries, which operate at room temperature and near neutral pH with high efficiency and high power density. The widely available metal and chelate materials coupled with the simple electrolyte synthesis provides a compelling pathway for expedited system scale-up. We anticipate that not only will this approach of utilizing chelates as a molecular barrier provide a general methodology to enable high-voltage aqueous batteries, but this inhibition of hydrogen evolution will carry wider implications for managing water splitting in other electrochemical applications.

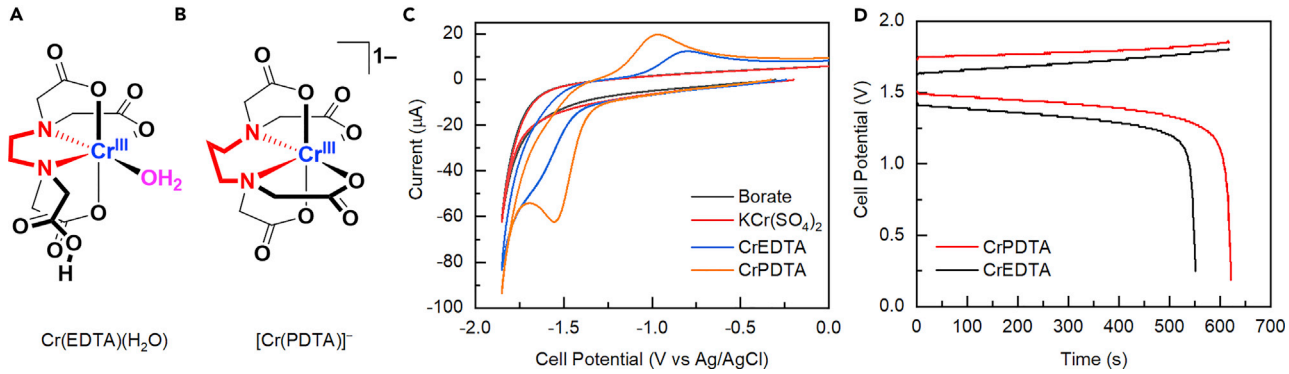

Figure 1. Chelate Structures and Electrochemical Behavior

(A) Molecular structure of Cr(EDTA)(H_2O) based on X-ray crystal structure data.

(B) Molecular structures of $[CrPDTA]^-$ based on X-ray crystal structure data; the change in N–N spacer is highlighted in red.

(C) CV data at 100 mV s^{-1} on a glassy carbon electrode for 0.125 M KB_i (pH 9) (black), uncomplexed 5 mM Cr(III) sulfate in 0.125 M KB_i (pH 9) (red) is insoluble under these conditions, 5 mM CrEDTA in 0.125 M KB_i (pH 9) (blue), and 5 mM CrPDTA in 0.125 M KB_i (pH 9) (orange).

(D) Single cycle bulk electrolysis at $\pm$0.1 A cm^{-2} of 0.4 M CrEDTA in 0.2 M KB_i (black) and 0.4 M CrPDTA in 0.2 M KB_i (red) versus 0.3 M $Fe(CN)_6^{4-}$ and 0.45 M $Fe(CN)_6^{3-}$ in 0.025 M KB_i.

using CrEDTA for both negative and positive redox couples was reported; however, the energy density was low (0.2 M concentration) and the overall energy efficiency was less than 7%.[9,10]

RESULTS

We hypothesized that the coordination of water to CrEDTA, which has been suggested by NMR, spectroscopic, and X-ray structural analysis[19–22] (Figure 1A) could be facilitating a catalytic pathway for water splitting, in a similar fashion to known molecular hydrogen evolution catalysts.[23] In contrast with CrEDTA, the related chelate 1,3-propylenediaminetertaacetic acid (PDTA) has been shown to complex Cr^{3+} ions in a nearly octahedral geometry (Figure 1B) and exclude water from the primary coordination sphere.[24] The $Cr^{3+/2+}$ reduction potential of CrPDTA (−1.10 V versus SHE) is also more negative than CrEDTA (Figure 1C) and appears to have improved electrode kinetics on a glassy carbon electrode, suggesting increased battery voltage and performance when used as a negative electrolyte.[17] Cyclic voltammetry (CV) of an aqueous solution containing CrPDTA in a potassium tetraborate (KB_i) buffer shows a reduction at −1.31 V versus. Ag/AgCl and kinetic analysis provided a diffusion coefficient $D_O = 6.2 \times 10^{-6}$ cm^2 s^{-1} and a reduction rate constant $k^0 = 1.7 \times 10^{-4}$ cm s^{-1} on glassy carbon (Figure S1 and Table S1), which suggests that CrPDTA diffuses freely in solution and can be reduced faster than aqueous $Cr^{3+/2+}$ and $V^{3+/2+}$ but slower than some organics.[25–27] Using a carbon paper electrode, the CV in Figure S2 suggests better reversibility than on glassy carbon, but because of the variability and unknown surface area of carbon paper, these electrodes could not be used for quantitative analyses. The CV data was further supplemented by electrolysis of a CrEDTA solution, which resulted in only 88% current efficiency over a single 20-min charge-discharge cycle (Figure 1D).

Iron-Chromium Flow Battery

We first investigated the electrochemical behavior of CrPDTA as an electrolyte paired with $K_4Fe(CN)_6$, which is an inexpensive and robust positive electrolyte used in other flow battery systems.[28] Extended CV cycling and aging of solutions containing both CrPDTA and $Fe(CN)_6$ suggest these two complexes can exist in solution as spectators without degradative reaction or precipitation (Figures 2A, S3,

[1]Department of Chemistry, University of Colorado Boulder, Boulder, CO 80309, USA

[2]Department of Chemical and Biological Engineering, University of Colorado Boulder, Boulder, CO 80309, USA

[3]Renewable and Sustainable Energy Institute, University of Colorado Boulder, Boulder, CO 80309, USA

[4]Lead Contact

*Correspondence: michael.marshak@colorado.edu

https://doi.org/10.1016/j.joule.2019.07.002

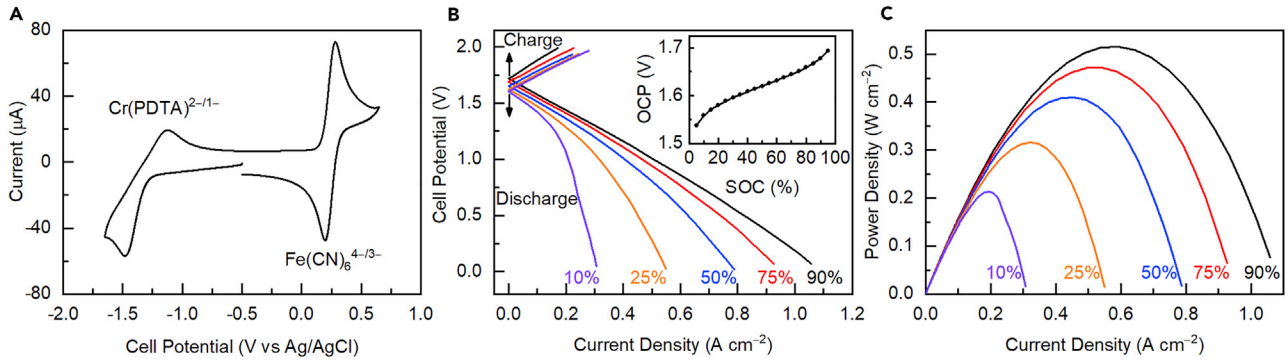

Figure 2. Iron-Chromium Cell Power Data

(A) CV at 100 mV s^{-1} of 5 mM KCrPDTA and 5 mM $K_4Fe(CN)_6$ in 0.125 M KB_i (pH 9) recorded on a glassy carbon working electrode.

(B) Polarization curves of a RFB containing 0.4 M CrPDTA in 0.2 M KB_i versus 0.3 M $Fe(CN)_6^{4-}$ and 0.45 M $Fe(CN)_6^{3-}$ in 0.025 M KB_i at varying SOC. See also Figure S8. Inset: cell OCP versus SOC.

(C) Discharge power density versus current density at varying SOC for solution from (B). See also Figure S8.

and S4).[29] Thus, the permeation of either species through the membrane should not decrease the cell performance beside the loss in storage capacity.

A bulk electrolyte solution of 0.4 M K[CrPDTA] was prepared by heating chrome alum with PDTA in the presence of KOH and buffered at pH 9.5 with 0.2 M KB_i. In order to evaluate the performance and stability of the negative electrolyte, the positive electrolyte was prepared with a volumetric excess of both $K_3Fe(CN)_6$ and $K_4Fe(CN)_6$ (0.75 M total Fe conc.) and buffered with 25 mM KB_i. These solutions were pumped through a flow cell containing carbon paper electrodes separated by a cation exchange membrane (Nafion 212). The cell was charged at 50 mA cm^{-2} and the open-circuit potential (OCP) monitored as a function of state of charge (SOC) from 5% to 95% (Figure 2B, inset). The OCP increased from 1.54 to 1.70 V, with a value of 1.62 V at 50% SOC; however we note the cell voltage response is slightly influenced by the large excess $Fe(CN)_6^{4-/3-}$ used as the positive electrolyte solution. The current-voltage behavior of the cell was monitored at various SOC values (Figure 2B) and shows nearly linear (i.e., ohmic) response between 1.2 and 2.0 V at 50% SOC, suggesting the cell performance is not substantially hindered by CrPDTA redox kinetics[30] but rather by the membrane resistance (total ohmic resistance = 1.7 Ω cm^2). The observed resistance is higher than other systems utilizing this same membrane and likely the result of the rather low K^+ ion concentration (0.8 M of the anolyte solution) of this non-optimized electrolyte formulation. Despite the high cell resistance, the cell voltage enables high discharge power density shown in Figure 2C, ranging from 0.2 to 0.5 W cm^{-2} between 10% and 90% SOC, with a peak power of 0.515 W cm^{-2}.

The cell was cycled 75 times at room temperature over 26 h at a constant current of ±0.1 A cm^{-2} using 80% of the total electrolyte capacity as a coulombic charging limit per cycle (Figure 3A). Under these conditions, the current efficiency per cycle was quantitative within measurement error (100.0% ± 0.3%) indicating no significant side reactions or hydrogen evolution occurred. The round-trip energy efficiency was 80.0% ± 0.4%, and the discharge capacity was unchanged from the first to the last cycle. Cycling to 90% SOC at 50 and 20 mA cm^{-2} reduced the overpotential, raising the round-trip energy efficiencies to 90% and 93%, respectively (Figure S5 and Table S2).

We increased the concentration of the CrPDTA electrolyte to 1.0 M and cycled the cell 25 times at 40°C (Figures 3B and 3C). Again, we observed quantitative current

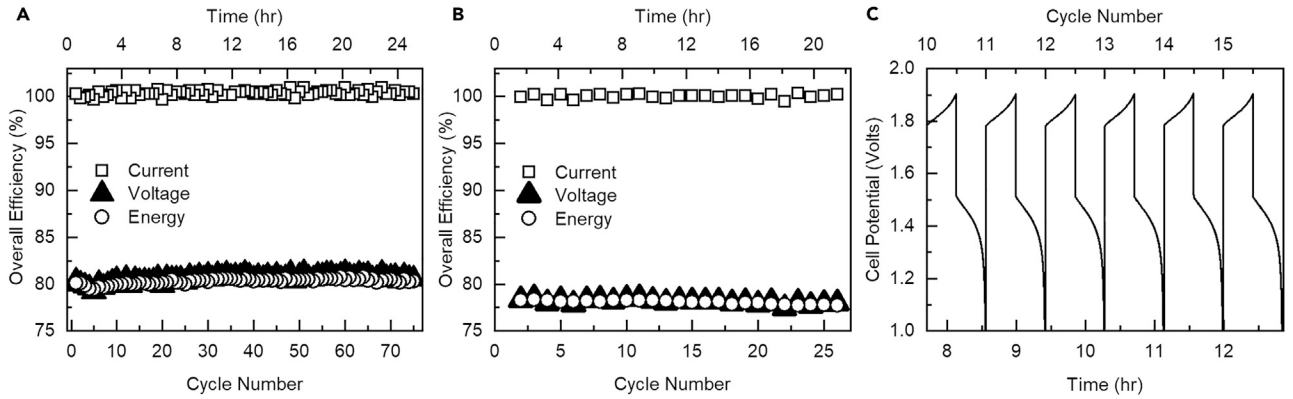

Figure 3. Iron-Chromium Chelate Cell Cycling Data

(A) Current, voltage, and energy efficiency per cycle at $\pm$0.1 A cm^{-2} to 80% SOC using 0.4 M CrPDTA in 0.2 M KB_i versus 0.3 M $Fe(CN)_6^{4-}$ and 0.45 M $Fe(CN)_6^{3-}$ in 0.025 M KB_i.

(B) Cell efficiencies per cycle for 25 cycles at $\pm$0.1 A cm^{-2} to 80% SOC using 1.0 M CrPDTA in 0.1 M KB_i versus 0.4 M $Fe(CN)_6^{4-}$ and 0.6 M $Fe(CN)_6^{3-}$ in 0.025 M KB_i.

(C) Cell voltage during cycling from (B).

efficiency (100% $\pm$ 0.2%), although the energy efficiency was 78.1% $\pm$ 0.2%. The maximum solubility of KCrPDTA at room temperature was observed to be 1.32 M; therefore, significant opportunities are available for improving the CrPDTA electrolyte to optimize concentration, viscosity, and performance, as has been shown for the $Fe(CN)_6$ electrolyte.[31]

During battery testing, we observed that increasing the maximum SOC from 80% to 90% resulted in a decrease in current efficiency to 99.5% $\pm$ 0.2% (Figures S6 and S7A), which we attribute to H_2 evolution at the electrode at the end of charging (Figure S6B). In order to evaluate the stability of the CrPDTA electrolyte in isolation from the electrode, a fully charged 0.4 M CrPDTA solution was transferred to a separate, sealed, argon-filled flask and evaluated by analyzing the headspace via gas chromatography. H_2 was observed after standing for one week; however, it amounted to an equivalent capacity loss of 2.7% or 0.4% per day. Depending on pH, the reduced CrPDTA electrolyte has a thermodynamic driving force of 500 to 600 mV with respect to the reversible hydrogen electrode, thus we hypothesize that trace metal impurities in the solution due to impurities in the starting reactants could be catalyzing hydrogen evolution. We have observed the reduced CrPDTA solution to rapidly evolve hydrogen when contacted with stainless steel, suggesting that trace metals could account for the relatively small amounts of hydrogen evolution that were observed. During the cycling experiment in Figure 3A, the electrolyte pH of CrPDTA increased from 9.5 to 10.0, which would equate to a current efficiency loss of 0.1% per cycle if attributed exclusively to H_2 evolution. Because quantitative current efficiency was observed during cycling, the pH increase could instead be caused by crossover of KB_i or exposure of reduced CrPDTA to O_2 before or after cycling to form OH^-. The reactivity with O_2 could initially form superoxide O_2^-, which is favored by 940 mV and could proceed by a kinetically facile outer sphere electron transfer mechanism.[32]

Decomposition of CrPDTA was not observed during testing, and the final discharge capacity was unchanged in each cycling experiment. The Pourbaix diagram for aqueous chromium suggests that any free chromium ions would not only form insoluble $Cr(OH)_3$ (K_{sp} = 10^{-30})[33] but would further be reduced to Cr^0 at the $-$1.1 V

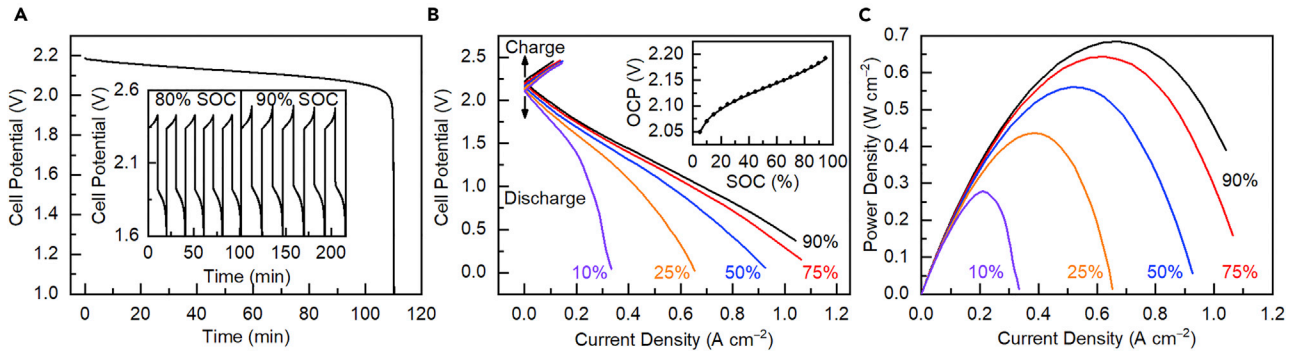

Figure 4. Chromium-Bromine Cell Cycling Data

(A) Cell potential during 10 mA cm^{-2} discharge from 90% SOC of 0.4 M CrPDTA in 0.2 M KB_i versus 2.0 M KBr and 0.5 M Br_2 in 0.1 M KB_i. Inset: cell potential during cycles at $\pm$0.1 A cm^{-2} to 80% and 90% SOC.

(B) Cell polarization curves at varying SOC. See also Figure S9. Inset: cell OCP versus SOC.

(C) Power density versus current density at varying SOC. See also Figure S9.

potential of the reduced CrPDTA electrolyte. Given the strong binding constants for EDTA to both Cr^{3+} (23.4) and Cr^{2+} (13.6),[34] we expect that the complexed Cr ions are substantially favored thermodynamically over the free ion.[35] Although very slow decomposition cannot be ruled out without long-term durability studies, we note that EDTA is considered a persistent organic chemical that decomposes primarily through exposure to UV radiation.[36] We would anticipate that any decomposition of PDTA would also be accompanied by the precipitation of Cr^{3+} ions as $Cr(OH)_3$ at pH 9, which was not observed, but any potential degradation could be mitigated by the addition of excess PDTA to the electrolyte solution. Because of the size and negative charge of CrPDTA, permeability through the cation exchange membrane is disfavored in comparison with positively charged metal ions. Nevertheless, improvement and optimization of membrane performance could provide improved stability given a static crossover experiment showed a rate of 0.01 mA cm^{-2}.

Chromium-Bromine Flow Battery

Because the CrPDTA redox couple operates near the negative limit of H_2 evolution on carbon, a redox couple more positive than $Fe(CN)_6^{3-/4-}$ is required to further increase the battery voltage. Therefore, the Br_2/Br^- redox couple was chosen to produce an RFB with a potential over 2.1 V. Figure 4A shows the discharge curve of a chromium-bromine (CrBr) RFB, wherein the cell maintains an operating voltage above 2 volts for nearly the complete discharge time. Cycling at $\pm$0.1 A cm^{-2} to both 80% and 90 % SOC results in stable charge-discharge cycles (Figure 4A, inset) with 97% current efficiency and an overall energy efficiency of 76% per cycle (Figure S7B). Since the previous cycling tests showed quantitative current efficiency with CrPDTA, the lower current efficiency here is attributed mostly to crossover of bromine through the membrane (1.5 mA cm^{-2}), which has been observed at a similar rate in other systems utilizing Nafion 212.[37,38] Cell polarization curves are reported in Figure 4B (total ohmic resistance = 2.93 Ω cm^2), and the OCP ranged from 2.05 to 2.2 V between 5% and 95% SOC (Figure 4B, inset). The peak power ranged from over 0.2 to 0.6 W cm^{-2}, with a maximum of 0.684 W cm^{-2} observed at 90% SOC (Figure 4C).

DISCUSSION

These results demonstrate two high-performance aqueous RFBs with higher operating voltages than all but a few reported non-aqueous or hybrid RFB systems.[39,40]

Aqueous electrolytes are often claimed to be limited by the water splitting potential (1.23 V); however, this voltage only represents the thermodynamic stability window, determined by the relationship $\Delta G_f = -nFE^0$. The ΔG_f of water (−237 kJ/mol) is negative, implying that the recombination of O_2 and H_2 is favorable. This thermodynamic driving force provides an opportunity to mitigate electrolyte decomposition (i.e., water splitting) through the use of pH rebalancing cells.[41]

In contrast with the thermodynamic limit, the kinetic working window of water can be significantly larger than 1.23 V, as it depends on the varying activation energy required for different water splitting reaction pathways. Thus, the ability to deliver high aqueous cell voltages is primarily a kinetic phenomenon. Li-ion batteries are able to operate at high voltages in part because partial electrolyte decomposition forms a corrosion layer called a solid-electrolyte interphase (SEI) that protects the electrolyte from further contact with the electrode.[42,43] Aqueous systems such as "water-in-salt" Li-ion batteries can similarly impart kinetic barriers to water splitting using ion-based SEIs and operate with cell potentials up to 4.0 V.[42] Here, we have demonstrated that a robust organic chelate, PDTA, can act as a "molecular SEI" to exclude water from binding to reactive Cr^{2+} ions, rendering them inert to water splitting reactions.

In a flow battery, hydrogen evolution can be catalyzed by heterogeneous and homogeneous pathways. Heterogeneous H_2 evolution occurs at the electrode, which in this case can depend on the morphology of the carbon, surface defects, and impurities. We have shown (Figures 1C and S2) that utilization of carbon as an electrode does not catalyze significant hydrogen evolution at pH 9 within 100 mV of the CrPDTA reduction potential. Homogeneous H_2 evolution occurs in solution, catalyzed by the redox-active species or other impurities in the electrolyte. The coordination of water or protons to a metal ion is usually considered to be one of the first mechanistic steps in both anodic and cathodic processes in water splitting. Furthermore, it has been shown that basic functional groups in close proximity to a metal, such as the free carboxylate arm in CrEDTA, can have dramatic effects on the rate of homogeneous electrocatalysis to form hydrogen.[23] The simple change from EDTA to PDTA emphasizes how critical understanding of the coordination structure at the atomic level can have outsized consequences in redox flow battery performance. This work also demonstrates the importance of the proper synthetic methodology required to ensure that the chelate forms strong interactions with the metal ion in all accessed redox states and that all metal ions are fully complexed, especially given that uncomplexed or partially complexed ions can plate out on the electrode, precipitate from solution, form insoluble Prussian blue complexes with $Fe(CN)_6$, or catalyze water splitting reactions.

The reported batteries cycled with high current efficiency in a buffered solution around pH 9. This pH was chosen, in part, because hydrogen evolution at the carbon electrode becomes increasingly facile both thermodynamically and kinetically as the electrolyte solution becomes more acidic. In addition, preliminary results suggest that above a pH of 11, CrPDTA is less stable, leading to decreases in cell efficiency. Because a pH of 9 implies a proton concentration of 10^{-9}, even very small amounts of hydrogen evolution can have outsized effects on the pH and drive the electrolyte outside the window of CrPDTA stability. The fact that the cell containing 1.0 M electrolyte was cycled repeatedly for nearly a day implies that hydrogen evolution from the electrolyte has been nearly eliminated. Nevertheless, we acknowledge the need for long-term cell cycling to better quantify electrolyte durability and other key cell metrics. To this end, we envision that the use of a small electrolyzer cell attached to

the CrPDTA electrolyte that splits water to generate O_2 (separate compartment) and drives protons through a membrane and into the CrPDTA solution could mitigate any slow pH increases and keep the electrolyte within the stable pH range for CrPDTA.

Conclusion

The CrPDTA electrolyte addresses many of the current limitations of other RFB chemistries and offers a new pathway to dramatically lower the cost of grid-scale energy storage.[3] We have demonstrated the ability of a chelated metal complex to enhance redox potential, solubility, stability, and electron transfer kinetics. Two high-performance and high-voltage RFBs are reported, including the highest ever reported all-aqueous non-hybrid RFB voltage at 2.13 and a 1.62 V RFB that cycles repeatedly over one day with nearly quantitative current efficiency indicating negligible H_2 generation or capacity loss. These RFBs use the low-cost inorganic materials iron, chromium, and bromine and a widely available organic chelating agent, and operate near neutral pH instead of in corrosive acid allowing for the use of less expensive tanks, pumps, and other system-level materials.

A comprehensive cost model would require further optimization in electrolyte formulation, in addition to a detailed manufacturing strategy and integrated systems analysis. Nevertheless, the use of CrPDTA should enable more rapid market penetration of this RFB electrolyte chemistry than many organic electrolytes because EDTA and related chelates are already commodity chemicals manufactured on a scale of 10^8 kg yr^{-1} for fertilizer, water treatment, and consumer products.[44]

More generally, we have demonstrated that control of the primary coordination of a metal complex through the use of inexpensive mass-produced chelates can kinetically stabilize aqueous flow batteries at potentials in large excess of the thermodynamic water splitting potential. The reduction potential of CrPDTA is −0.57 V versus the reversible hydrogen electrode at pH 9, which is significantly beyond previously established aqueous stability limits.[2,8] We anticipate that the molecular inhibition of water splitting using chelates not only will provide a general approach in imparting kinetic stability to high-voltage aqueous batteries but also will carry wider implications for managing H_2 evolution in other electrochemical applications.

EXPERIMENTAL PROCEDURES

Electrolyte Preparation

$K_3Fe(CN)_6$, $K_4Fe(CN)_6$, KOH, KBr, Br_2, and $K_2B_4O_7$ were purchased from either Alfa Aesar or Acros and used as received. K[CrPDTA] was prepared via a modified version of a method described in literature.[45] A diagram of the chemical reaction to produce K[CrPDTA] and the following potassium sulfate removal is shown as Figure S10. $KCr(SO_4)_2 \cdot 12H_2O$ (40 g, 80 mmol, Acros, 98+%) and 1,3-diaminopropane-*N*,*N*,*N*′,*N*′-tetraacetic acid (27.5 g, 90 mmol, Sigma Aldrich, 99%) were dissolved in 30 mL of deionized water and heated to 100°C. After 1 h of heating, solid KOH (10 g) was added in 0.5 gram increments every 15 s. After 24 h, 16 mL of 5 M KOH was added slowly in 1 mL increments. Another 16 mL of 5 M KOH was added after an additional 24 h of heating. The pH of the solution was monitored during the addition of KOH and kept below 2.5 until after 48 h of heating. After 72 h of total reaction time, the final solution pH was between 5 and 6. The solution was cooled to room temperature, and 95 mL of acetone was added, precipitating solid K_2SO_4, which was removed by filtration. The filtrate was concentrated under reduced pressure to produce a stock solution. The flow cell was run at concentrations of 0.4 M and 1.0 M K[CrPDTA]. 0.4 M K[CrPDTA] solutions were created by diluting

the stock solution with deionized (DI) water to 10 mL and adding $K_2B_4O_7 \cdot 4\,H_2O$ (0.6 g, 2 mmol) to yield an electrolyte containing 0.4 M K[CrPDTA] and 0.2 M $K_2B_4O_7$ at pH 9.5. 1.0 M K[CrPDTA] solutions were created by diluting saturated K[CrPDTA] at 40°C with DI water to 10 mL and adding $K_2B_4O_7 \cdot 4\,H_2O$ (0.3 g, 1 mmol) to yield an electrolyte containing 1.0 M K[CrPDTA] and 0.1 M $K_2B_4O_7$ at pH 9.0. The CrEDTA solution was prepared in the same manner with H_4EDTA substituted for H_4PDTA.

Solubility Measurement

The concentration of CrPDTA was assessed by absorption spectroscopy using the absorbance at 506 nm (ε = 116 M^{-1} cm^{-1}).[18] UV-vis spectrophotometry measurements were performed using an AvaSpec-UL2048(L) unit.

Half-Cell Measurements

CV was conducted using a Gamry Interface 1000 potentiostat, an Ag/AgCl aqueous reference electrode (3 M NaCl filling solution), a Pt wire counter electrode, and a 3-mm-diameter glassy carbon electrode. Half-cell experiments were conducted on a solution containing 5 mM K[CrPDTA], 5 mM $K_4Fe(CN)_6$, and 0.125 M $K_2B_4O_7$ at pH 9. Solutions were first purged with N_2 and then kept under a blanket of argon while tests were performed. For carbon paper CV experiments, the same setup was used with the glassy carbon electrode swapped out for a piece of carbon paper.

Flow Cell Measurements

A 5 cm^2 single-cell flow battery was purchased from Fuel Cell Technologies Inc. with the acid cell configuration, so that the tubing carrying the electrolyte feeds directly into the graphite flow plate without contacting the aluminum or stainless-steel cell components. The flow plates comprised Poco graphite blocks with 5 cm^2 single serpentine flow fields. The $K_4Fe(CN)_6$ and CrPDTA electrolytes were contained in 100 mL round bottom flasks fitted with a rubber septum with holes drilled for 1/8″ OD perfluroacetoxy (PFA) inlet/outlet tubing. The KBr electrolyte was contained in a 60 mL PFA column component vessel capped with a 58 mm transfer closure with two 1/8″ OD compression fitting ports (Savillex). The $K_4Fe(CN)_6$ electrolyte was pumped into and out of the flow cell at a rate of 50 mL min^{-1} with a gear pump (Cole-Parmer) using 1/8″ OD, 1/16″ ID PFA tubing and PFA compression fittings. Due to the reactivity of Cr(II)PDTA and Br_2 solutions with stainless steel, a polytetrafluoroethylene (PTFE) diaphragm pump (Cole-Parmer) was used to pump into and out of the flow cell at an average flow rate of 42 mL min^{-1} and also used 1/8″ OD, 1/16″ ID PFA tubing and PFA compression fittings. Flow cell experiments were conducted using a Gamry Interface 5000E potentiostat/galvanostat.

Flow Cell Material Preparation and Assembly

A Nafion 212 membrane (50 μm thick, 3 × 3 cm) was soaked in DI water for a minimum of 12 h and gasketed with a 0.002″ PTFE sheet. Five stacked sheets (280 μm thick and 5 cm2 each) of GDL 39 AA carbon paper (SGL) were heated to 150°C in air for 12 h and used on each side with a 0.04″ PTFE gasket providing 27% compression. The cell was bolted together and tightened with a torque wrench to 10 N m.

Pulse Dampening

As further explained in the Supplemental Experimental Procedures, the diaphragm pumps created pulsed data during the power generation experiments due to the pulsed flow. As shown in Figures S8, S9, 2B, 2C, 4B, and 4C were generated by fitting lines to the original pulsed data. All other figures, including those used for efficiency calculations and to show cycling, were generated with the original data as no fluctuations were observed at the lower current densities.

DATA AND CODE AVAILABILITY

Full data available upon request from the authors.

SUPPLEMENTAL INFORMATION

Supplemental Information can be found online at https://doi.org/10.1016/j.joule.2019.07.002.

ACKNOWLEDGMENTS

We thank J.R. Bertram and Prof. P. Nagpal for allowing us to use their gas chromatograph; Jona Koka, Hunter Wood, and Miguel Coto for assistance with electrolyte synthesis; Franklin Maharaj for assistance with electrochemical testing; and Aaron Crossman for assistance with electrolyte purification. This work was funded by startup and seed funding from the University of Colorado Boulder. B.H.R. was supported, in part, by a Graduate Assistance in Areas of National Need (GAANN) Fellowship from the U.S. Department of Education.

AUTHOR CONTRIBUTIONS

B.H.R. synthesized electrolyte formulations and performed all experiments in the manuscript. J.M.F. synthesized electrolyte formulations and assisted in performing initial chelate screening. M.P.M. conceived and supervised this project. B.H.R., J.M.F., and M.P.M. collectively wrote this manuscript.

DECLARATION OF INTERESTS

The University of Colorado has filed a patent on some of the intellectual property disclosed in this manuscript.

Received: April 10, 2019
Revised: May 3, 2019
Accepted: July 2, 2019
Published: July 25, 2019

REFERENCES

1. Annual Energy Outlook 2019. U.S. (2019) (Energy Information Administration).
2. Yang, Z., Zhang, J., Kintner-Meyer, M.C.W., Lu, X., Choi, D., Lemmon, J.P., and Liu, J. (2011). Electrochemical energy storage for Green Grid. Chem. Rev. *111*, 3577–3613.
3. Soloveichik, G.L. (2015). Flow batteries: current status and trends. Chem. Rev. *115*, 11533–11558.
4. Vesborg, P.C.K., and Jaramillo, T.F. (2012). Addressing the terawatt challenge: scalability in the supply of chemical elements for renewable energy. RSC Adv. *2*, 7933–7947.
5. Ponce de León, C., Frías-Ferrer, A., González-García, J., Szánto, D.A., and Walsh, F.C. (2006). Redox flow cells for energy conversion. J. Power Sources *160*, 716–732.
6. Zeng, Y.K., Zhao, T.S., An, L., Zhou, X.L., and Wei, L. (2015). A comparative study of all-vanadium and iron-chromium redox flow batteries for large-scale energy storage. J. Power Sources *300*, 438–443.
7. Skyllas-Kazacos, M., Rychcik, M., Robins, R.G., Fane, A.G., and Green, M.A. (1986). New all-vanadium redox flow cell. J. Electrochem. Soc. *133*, 1057–1058.
8. Chalamala, B.R., Soundappan, T., Fisher, G.R., Anstey, M.R., Viswanathan, V.V., and Perry, M.L. (2014). Redox flow batteries: an engineering perspective. Proc. IEEE *102*, 976–999.
9. Bae, C.-H., Roberts, E.P.L., and Dryfe, R.A.W. (2002). Chromium redox couples for application to redox flow batteries. Electrochim. Acta *48*, 279–287.
10. Bae, C., Roberts, E.P.L., Chakrabarti, M.H., and Saleem, M. (2011). All-chromium redox flow battery for renewable energy storage. Int. J. Green Energy *8*, 248–264.
11. Modiba, P., Matoetoe, M., and Crouch, A.M. (2013). Kinetics study of transition metal complexes (Ce–DTPA, Cr–DTPA and V–DTPA) for redox flow battery applications (Ce–DTPA, Cr–DTPA, and V–DTPA). Electrochim. Acta *94*, 336–343.
12. Chen, Y.-W.D., Santhanam, K.S.V., and Bard, A.J. (1981). Solution redox couples for electrochemical energy storage II. Cobalt(III)-Cobalt(II) complexes with o-phenanthroline and related ligands. J. Electrochem. Soc. *128*, 1460–1467.
13. Ibanez, J.G., Choi, C.-S., and Becker, R.S. (1987). Aqueous redox transition metal complexes for electrochemical applications as a function of pH. J. Electrochem. Soc. *134*, 3083–3089.
14. Mori, Y., and Yokoi, H. (1994). Studies on the interaction between iron(III) and glycerol or related polyols over a wide pH range. Bull. Chem. Soc. Jpn. *67*, 2724–2730.
15. Wen, Y.H., Zhang, H.M., Qian, P., Zhou, H.T., Zhao, P., Yi, B.L., and Yang, Y.S. (2006). A study of the Fe(III)/Fe(II)–triethanolamine complex redox couple for redox flow battery application. Electrochim. Acta *51*, 3769–3775.
16. Hawthorne, K.L., Wainright, J.S., and Savinell, R.F. (2014). Studies of iron-ligand complexes for an all-iron flow battery application. J. Electrochem. Soc. *161*, A1662–A1671.
17. Ogino, H., Nagata, T., and Ogino, K. (1989). Redox potentials and related thermodynamic parameters of (diaminopolycarboxylato)

metal(III/II) redox couples. Inorg. Chem. *28*, 3656–3659.

18. Hecht, M., Schultz, F.A., and Speiser, B. (1996). Ligand structural effects on the electrochemistry of chromium(III) amino carboxylate complexes. Inorg. Chem. *35*, 5555–5563.

19. Pecsok, R.L., Shields, L.D., and Schaefer, W.P. (1964). Complexes of chromium (II) and (III) with ethylenediaminetetraacetic acid. Inorg. Chem. *3*, 114–116.

20. Thorneley, R.N.F., and Sykes, A.G. (1968). The extent of chelation in some chromium(III)-EDTA complexes. Chem. Commun. (London), 340–341.

21. Gerdom, L.E., Baenziger, N.A., and Goff, H.M. (1981). Crystal and molecular structure of a substitution-labile chromium(III) complex: aquo(ethylenediaminetriacetatoacetic acid) chromium(III). Inorg. Chem. *20*, 1606–1609.

22. Wheeler, W.D., and Legg, J.I. (1984). Solution structure of the chromium(III) complex with EDTA by deuteron NMR spectroscopy. Inorg. Chem. *23*, 3798–3802.

23. Helm, M.L., Stewart, M.P., Bullock, R.M., DuBois, M.R., and DuBois, D.L. (2011). A synthetic Nickel electrocatalyst with a turnover frequency above 100,000 s−1 for H_2 production. Science *333*, 863–866.

24. Herak, R., Srdanov, G., Djuran, M.I., Radanović, D.J., and Bruvo, M. (1984). Crystal structures of Na[M(1,3-PDTA)]·3H2O(M = Cr, Rh; 1,3-PDTA = 1,3-propanediaminetetraacetate), and the absolute configuration of the (-)D-isomer of the Rh complex. Inorg. Chim. Acta *83*, 55–64.

25. Randles, J.E.B., and Somerton, K.W. (1952). Kinetics of rapid electrode reactions. Trans. Faraday Soc. *48*, 11.

26. Sum, E., and Skyllas-Kazacos, M. (1985). A study of the V(II)/V(III) redox couple for redox flow cell applications. J. Power Sources *15*, 179–190.

27. Huskinson, B., Marshak, M.P., Suh, C., Er, S., Gerhardt, M.R., Galvin, C.J., Chen, X., Aspuru-Guzik, A., Gordon, R.G., and Aziz, M.J. (2014). A metal-free organic–inorganic aqueous flow battery. Nature *505*, 195–198.

28. Lin, K., Chen, Q., Gerhardt, M.R., Tong, L., Kim, S.B., Eisenach, L., Valle, A.W., Hardee, D., Gordon, R.G., Aziz, M.J., et al. (2015). Alkaline quinone flow battery. Science *349*, 1529–1532.

29. Darling, R., Gallagher, K., Xie, W., Su, L., and Brushett, F. (2016). Transport property requirements for flow battery separators. J. Electrochem. Soc. *163*, A5029–A5040.

30. Sun, C.-N., Delnick, F.M., Aaron, D.S., Papandrew, A.B., Mench, M.M., and Zawodzinski, T.A. (2013). Probing electrode losses in all-vanadium redox flow batteries with impedance spectroscopy. ECS Electrochem. Lett. *2*, A43–A45.

31. Esswein, A.J., Goeltz, J., and Amadeo, D. (2014) High solubility iron hexacyanides. US20140051003A1.

32. Wood, P.M. (1988). The potential diagram for oxygen at pH 7. Biochem. J. *253*, 287–289.

33. Bard, A.J., Parsons, R., and Jordan, J. (1985). Standard potentials in aqueous solution (CRC Press).

34. Harris, D.C. (2007). Quantitative chemical analysis, 3rd Printing, Seventh edition (W. H. Freeman).

35. Ogino, H., Chung, J.-J., and Tanaka, N. (1971). On the utilization of chromium(II) ions for the syntheses of alkylenediaminetetraacetatochromate(III) complexes. Inorg. Nucl. Chem. Lett. *7*, 125–129.

36. Bucheli-Witschel, M., and Egli, T. (2001). Environmental fate and microbial degradation of aminopolycarboxylic acids. FEMS Microbiol. Rev. *25*, 69–106.

37. Tucker, M.C., Cho, K.T., Spingler, F.B., Weber, A.Z., and Lin, G. (2015). Impact of membrane characteristics on the performance and cycling of the Br_2–H_2 redox flow cell. J. Power Sources *284*, 212–221.

38. Chen, Q., Eisenach, L., and Aziz, M.J. (2016). Cycling analysis of a quinone-bromide redox flow battery. J. Electrochem. Soc. *163*, A5057–A5063.

39. Stauber, J.M., Zhang, S., Gvozdik, N., Jiang, Y., Avena, L., Stevenson, K.J., and Cummins, C.C. (2018). Cobalt and vanadium trimetaphosphate polyanions: synthesis, characterization, and electrochemical evaluation for non-aqueous redox-flow battery applications. J. Am. Chem. Soc. *140*, 538–541.

40. Walsh, F.C., Ponce de Léon, C., Berlouis, L., Nikiforidis, G., Arenas-Martínez, L.F., Hodgson, D., and Hall, D. (2015). The development of Zn–Ce hybrid redox flow batteries for energy storage and their continuing challenges. ChemPlusChem *80*, 288–311.

41. Gahn, R.F., Hagedorn, N.H., and Johnson, J.A. (1985). Cycling performance of the iron-chromium redox energy storage system In the Proccedings of the 20th Intersociety Energy Conversion Energy Conference, Miami Beach, FL, United States.

42. Yang, C., Chen, J., Qing, T., Fan, X., Sun, W., von Cresce, A., Ding, M.S., Borodin, O., Vatamanu, J., Schroeder, M.A., et al. (2017). 4.0 V aqueous Li-Ion batteries. Joule *1*, 122–132.

43. Suo, L., Borodin, O., Gao, T., Olguin, M., Ho, J., Fan, X., Luo, C., Wang, C., and Xu, K. (2015). "Water-in-salt" electrolyte enables high-voltage aqueous lithium-ion chemistries. Science *350*, 938–943.

44. Hart, J.R. (2011). Ethylenediaminetetraacetic acid and related chelating agents. Ullmann's encyclopedia of industrial chemistry (Wiley-VCH Verlag GmbH & Co).

45. Pletcher, D., and White, J.C.P. (1992). Studies of indirect electrochemical reductions using chromium complexes with polyaminocarboxylate ligands as mediators. Electrochim. Acta *37*, 575–583.